



Gas Adsorption/Diffusion in Bidisperse Coal Particles: Investigation for an Effective Diffusion Coefficient in Coalbeds

J. YI

Chongqing University of Science and Technology

I. Y. AKKUTLU, C.V. DEUTSCH

University of Alberta

This paper is to be presented at the Petroleum Society's 7th Canadian International Petroleum Conference (57th Annual Technical Meeting), Calgary, Alberta, Canada, June 13 – 15, 2006. Discussion of this paper is invited and may be presented at the meeting if filed in writing with the technical program chairman prior to the conclusion of the meeting. This paper and any discussion filed will be considered for publication in Petroleum Society journals. Publication rights are reserved. This is a pre-print and subject to correction.

Abstract

Pore structure of coalbeds exhibits multi-scale heterogeneity. It is common practice to characterize the coalbeds using two distinctive porosity systems: a well-defined and uniformly distributed network of natural fractures, and nearly impermeable and non-uniform coal matrix blocks. The blocks consist of microporous solids with large internal surface area and strong affinity for some naturally occurring chemical species such as methane and carbon dioxide. At high coalbed pressures, therefore, these species exist abundantly and/or could be stored in large quantities at a physically adsorbed liquid-like state. Much work has been carried out on adsorption capacity of various coals. Diffusive transport processes within the matrix blocks could be the rate limiting step for adsorption during gas injection and production operations. Identifying these processes and determining their contributions to overall (upscaled) mass transport is a complex and time consuming procedure. The paper presents numerical diffusion models in varying coal particles and investigates transport mechanisms. For this purpose, the coal particle is represented as a microporous solid penetrated by a network of larger interconnected macropores. The solid consists of pores of the order of a few molecular diameters and adsorbs the bulk of the gas. A simple relationship between the apparent and intrinsic (macropore

and solid) Fickian diffusion coefficients is shown to exist in the case of single-component (methane) nonlinear Langmuir-type adsorption. Mass transport in the bidisperse coal particle is significantly influenced by adsorption in microporous solid. The investigation is then extended to study concentration dependence of the microporous solid diffusion for binary (methane-CO₂) mixtures. It is found that co-diffusion of the gas molecules enhances, while counter-diffusion diminishes the gas mass transport in the solid in the presence of competitive sorption dynamics. The isotherm nonlinearity effects and the influence of lateral interactions among the adsorbed molecules in the solid phase are discussed. A sensitivity analysis is given to identify conditions that promote desorbed methane production from and adsorbed CO₂ storage in the microporous solid. The work finds application in modeling CBM and ECBM processes.

1. Introduction

As an unconventional natural gas resource, coalbed methane receives worldwide attention. Deep coal seams that are not accessible for mining are suitable for in-situ gas production using conventional drilling, well completion and gas recovery technologies. Hence, a

vast amount of natural gas is globally available. Unlike the conventional gas resources, however, the gas storage, flow and transport processes in coalbeds are quite complex mainly due to an intricate nature of the coalbeds.

Coalbeds are porous media often characterized by a bimodal pore structure: a primary structure consisting of micro- and meso-scale pores, and a secondary structure with macropores and interconnected natural fractures. The microporous coal has extremely large internal surface area and strong affinity for certain naturally occurring chemical species such as methane, carbon dioxide, nitrogen and water. At high coalbed pressures, therefore, majority of the natural gas in-place, in particular methane, exists abundantly at an adsorbed liquid-like state in the microporous solid [1].

Depressurizing the coalbed yields a significant volume of natural gas. However, initial stage of recovery is dominated by water production, whereas the latter stage is under the influence of diffusional resistances of the primary pores of the coal matrix. Treatment and disposal of the produced water is expensive and its long-term environmental impact has not been clearly understood yet. Injection of a second gas with much higher adsorption capacity, on the other hand, could possibly enhance recovery by (1) maintaining the overall reservoir pressure, thus, keeping the water production at a minimum level; and (2) lowering the partial pressure of the coalbed methane in the migrating gas phase, hence, promoting methane desorption. It is predicted that methane recovery that could be achieved in this manner exceeds the recoveries using depressurization by a factor of 2-3. Consequently, carbon dioxide injection is being considered world-wide for enhanced coalbed methane production (CO₂-ECBM) and for the prospect of geological sequestration of CO₂ as the means of reducing global greenhouse gas emissions.

CO₂-ECBM involves phenomena of fundamental interest and raises challenging questions related to the chemically and structurally intricate nature of coalbeds [2]. Flow of injected CO₂ in the fracture network initiates several counter-diffusive and competitive adsorption processes between the molecules in tight coal matrix (macro-, meso- and micropores): molecular diffusion (dominated by molecule-molecule collisions), Knudsen diffusion (molecular streaming dominated by molecule-wall collisions) and surface diffusion (transport through the physically adsorbed layer). As the consequence of these processes, the incoming CO₂ molecules are expected to activate and displace the in-place methane molecules in the coal matrices.

The method involves three stages: (1) flow of gas, in particular in the fractures; (2) multi-component gas diffusive transport in the fractures and the matrices; and (3) competitive sorption phenomena in the matrices, in particular in the micropore structure. These simultaneously take place in the coalbeds within at least three different characteristic time and length scales, i.e., the scales of injector/producer well-spacing, of coal matrix bounded by the fractures and of the internal surface area of the micropores, respectively. In such a complex system, two possible scenarios could lead to early breakthrough of the injected CO₂, hence uneconomical sequestration and recovery. Competitive adsorption rates of the gas components could be controlled by the counter-diffusive mass fluxes of these components. According to this scenario, nature of the multi-component diffusive transport processes in the coal matrices should be understood clearly. Since the matrices consist of microporous

solid, thus, exhibit a large internal surface area for the sorption phenomena and a strong affinity for the gas mixture, it is quite natural to expect additional diffusive mass transport in both the adsorbed and free gas phases in the directions of CO₂ and methane mass fluxes. Contribution of these fluxes could vary spatially/temporally and they should be represented accurately in the computational models. It could then be impractical to determine an effective diffusion coefficient for the coal matrix blocks. Fundamental research on counter-diffusion and competitive adsorption in the coal matrix is, therefore, currently necessary.

On the other hand, according to the second scenario, gas storage and recovery could be controlled by the sorption phenomena taking place at the internal surfaces of the microporous solids. Then, gas injection and production in coalbeds could be optimized only if the nature of competitive gas sorption kinetics in coal matrices is well understood. The parameters of equilibrium sorption are relatively easy to determine in the laboratory, but the same cannot be claimed when nonlinear sorption kinetics become part of an investigation. Currently it remains an experimental and theoretical challenge to investigate sorption dynamics in heterogeneous coal matrices [2].

Gas flow and transport in coalbeds has been a subject of research for several decades. In accordance with the first scenario, the roles of diffusive transport and equilibrium adsorption on the overall methane release from the coal matrix to the fracture network has been considered previously. Investigations using coal particles first appeared to be suitable for this purpose, since the particles may not contain fractures yet it could still be represented by a multi-scale (macro- and micro-scale) pore structure. Unipore diffusion models are not suitable for this purpose, however, since these models consider a homogeneous pore structure at the macro-scale only and, hence, over predict gas desorption rates [3].

Ruckenstein *et al.* [4] theoretically considered single-component diffusion in a small bidisperse sorbent particle, i.e., spherical macroporous particle consisting of uniformly-distributed microporous solid spheres in continuum. In their case, the adsorptive/diffusive equation describing gas transport in the solid spheres is coupled to that for the macro-particle with an additional diffusional gas mass flux term. Later, their approach has been extended to model gas flow and transport in fixed beds by Smith and Williams [5] to investigate methane release rates in coalbeds, and more recently by Shi and Durucan [6] to study mechanisms of CO₂-enhanced methane recovery. The approach, although easy to apply and appears to be promising in terms of capturing the mechanisms of gas flow and transport in a multi-scale coalbed, emerges as a rather large problem involving several independent *a priori* transport coefficients, hence preventing rigorous engineering analysis.

The purpose of this paper is to develop a theoretical framework suitable for a fundamental investigation of single- and multi-component (binary) gas transport in the macropores and transport/storage in the microporous solid. For this, we consider a bidisperse coal particle viewed as a solid penetrated throughout by a network of larger interconnected pores, i.e., macropores. Initially, gas is distributed uniformly in an adsorbed liquid-like state in the solid that contains pores on the order of a few molecular diameters (< 20 Angstrom), and as free gas in the macropores. We consider that the solid adsorbs the bulk of the gas; while the macropores have relatively negligible gas adsorption capacity. Resistance controlling

the equilibrium adsorption dynamics is due to surface diffusion, i.e., adsorbed-phase diffusion in the micropores solid. The latter indicates that, although the adsorbed gas molecules are always under the restrictive influence of the solid phase, hence, their mobility is much smaller than that in the macropores; the concentrations in the adsorbed-phase are much higher so that significant surface fluxes are possible in the micropores. According to this view, the mass transport is similar to diffusion of a gas in porous polymers.

In the first part of the paper, we numerically investigate methane diffusion in helium carrier in the coal particle using a simpler theoretical approach that does not require solution of coupled differential equations as defined in references [4-6]. During the gas release from the particle, methane mass transport is only due to surface diffusion in the microporous solid and to molecular diffusion in the macropores. The two transport mechanisms are represented by Fickian diffusion with concentration-independent coefficients, D_{s0} and D_p respectively. (Later, in the multi-component case, the assumption of concentration independence of D_{s0} will be relaxed). Similar models, e.g., Gray and Do [7], have been used extensively in chemical engineering literature, in the context of acid gas separation in bimodal porous adsorbents such as zeolites and active carbon particles. Here, we follow a similar approach and study the roles of equilibrium methane sorption and transport mechanisms on an effective (overall) diffusion coefficient in varying types of coal particles.

Second part of the paper addresses issues related to the behavior of binary (methane-CO₂) gas mixtures in the coal particle; it investigates whether and how the presence of an additional gas component with a larger adsorption capacity could enhance methane recovery from the particle. Although competitive adsorption and diffusion are important for practical reasons, our understanding of the system dynamics is limited due to difficulties of measuring quantities related to mixture diffusion. Therefore, no precise experimental data are currently available to quantitatively validate some of the results and conclusions of this part of the work.

Theoretical framework for multi-component diffusion has been described by Cussler [8], where the general rules are summarized for deciding when strong diffusion effects are expected. Later, due to its importance in adsorption and catalysis, multi-component solid diffusion in microporous materials has been studied extensively. Mostly, the theoretical works in this area are in the form of a generalized Maxwell-Stefan problem based on the principles of irreversible thermodynamics [9] and predict the main term microporous solid diffusion coefficients from the experimental single-component data. The cross-term diffusion coefficients are then calculated from the main term coefficients using an empirical formula for the gas mixture. Yang and coworkers [10, 11] recently demonstrated how the pure component Fickian surface diffusivities can be used to predict diffusion of binary gas mixtures in microporous solids in the absence of macropore structure, i.e., ϕ is zero. In this study, their work is incorporated to investigate effective methane/CO₂ diffusion in bidisperse coal particles.

Since it retains majority of the gas in-place, focus of our analysis will be on the microporous solid phase. More specifically, we theoretically investigate the influences of adsorption and diffusion processes in the solid phase on the overall gas transport in coal particle. As will be shown, the challenge in this case is to predict and

investigate the roles of mechanisms in the solid phase on the overall transport in the coal particle. To achieve this, we suppress the role of macropore diffusion by fixing its coefficients (D_p , D_{p1} and D_{p2}) to constant values, and make observations regarding the mechanisms in the microporous solid phase using dimensionless quantities normalized by the latter.

2. Single Component Diffusion in Bi-disperse Coal Particle

Single-component gas diffusion experiments will be carried out numerically under isothermal conditions using dimensionless governing equations, which have been developed as follows.

Gas mass balance in a one-dimensional spherical bidisperse coal particle contains the following transient and diffusive terms:

$$\phi \frac{\partial C}{\partial t} + (1-\phi) \frac{\partial C_\mu}{\partial t} = \frac{1}{x^2} \frac{\partial}{\partial x} \left(\phi D_p x^2 \frac{\partial C}{\partial x} \right) + \frac{1}{x^2} \frac{\partial}{\partial x} \left((1-\phi) D_{s0} x^2 \frac{\partial C_\mu}{\partial x} \right) \quad (1)$$

Here, C is the free gas concentration in the macropores (mole per unit macropore volume), whereas C_μ represents concentration of the gas adsorbed by the microporous solid (mole per unit solid volume). The first terms on both sides of the governing equation include a constant macroporosity ϕ describing mass accumulation and diffusive mass flux of the gas in the macropore void space respectively; the second terms with the coefficient $(1-\phi)$, on the other hand, similarly represent the accumulation and transport in the microporous solid. Hence, bidisperse nature of the coal particle is introduced in single equation simply by defining accumulation and flux terms involving macropore and microporous solid volumes.

In addition, the solid is considered to be in equilibrium with the gas in the micropore and nonlinear Langmuir isotherm to describe physical adsorption. If $C_{\mu s}$ represent the complete monolayer coverage in the solid, then the equilibrium adsorption dynamics has previously been given as:

$$C_\mu = \frac{C_{\mu s} b' C}{1 + b' C} \quad (2)$$

Here $b' = bRT$ and b is often referred to as the Langmuir constant. When the total gas pressure p is low (i.e., $bp \ll 1$), equation (2) reduces to Henry's law isotherm, which states that the adsorbed gas concentration in the solid increases linearly with pressure [4]. The Langmuir model has been derived from both kinetic and statistical mechanical points of view under the assumptions of adsorption on a fixed number of sites that are energetically equivalent; and no lateral interactions exist between the adsorbed molecules on the neighboring sites.

With appropriate initial and boundary conditions, numerical solution to equations (1) and (2) can be obtained using the orthogonal collocation technique [7]. Here, we follow a different approach and convert equation (1) into the following format so that we not only obtain numerical solutions accurately and easily but also study existence and behavior of an effective diffusion coefficient D for the defined gas/solid system under initial and boundary conditions that will be specified later, in §5:

$$\frac{\partial C}{\partial t} = \frac{D}{x^2} \frac{\partial}{\partial x} \left(x^2 \frac{\partial C}{\partial x} \right) \quad (3)$$

Notice that the only dependent variable in equation (3) is the free-gas concentration $C(x,t)$ in the macropores and, hence, the effective diffusion coefficient must additionally include not only resistance due to gas transport in the microporous solid but also retardation due to adsorption.

Using the chain rule, equation (1) is first written in the following form:

$$\left[\phi + (1-\phi) \frac{\partial C_\mu}{\partial C} \right] \frac{\partial C}{\partial t} = \frac{1}{x^2} \frac{\partial}{\partial x} \left(\phi D_p x^2 \frac{\partial C}{\partial x} \right) + \frac{1}{x^2} \frac{\partial}{\partial x} \left[(1-\phi) D_{s0} x^2 \frac{\partial C_\mu}{\partial C} \frac{\partial C}{\partial x} \right] \quad (4)$$

Next, the last term on the right hand side of equation (4) is expanded as follows:

$$\left[\phi + (1-\phi) \frac{\partial C_\mu}{\partial C} \right] \frac{\partial C}{\partial t} = \frac{1}{x^2} \frac{\partial}{\partial x} \left(\phi D_p x^2 \frac{\partial C}{\partial x} \right) + \frac{1}{x^2} \frac{\partial C_\mu}{\partial C} \frac{\partial}{\partial x} \left[(1-\phi) D_{s0} x^2 \frac{\partial C}{\partial x} \right] + (1-\phi) D_{s0} \frac{\partial C}{\partial x} \frac{\partial}{\partial x} \left(\frac{\partial C_\mu}{\partial C} \right) \quad (5)$$

From equation (2) we have

$$\frac{\partial C_\mu}{\partial C} = \frac{C_{\mu s} b'}{(1+b'C)^2} \quad (6)$$

which, once substituted into equation (5), yields:

$$\left[\phi + \frac{(1-\phi) C_{\mu s} b'}{(1+b'C)^2} \right] \frac{\partial C}{\partial t} = \frac{1}{x^2} \frac{\partial}{\partial x} \left(\phi D_p x^2 \frac{\partial C}{\partial x} \right) + \frac{C_{\mu s} b'}{(1+b'C)^2} \frac{1}{x^2} \frac{\partial}{\partial x} \left[(1-\phi) D_{s0} x^2 \frac{\partial C}{\partial x} \right] + (1-\phi) C_{\mu s} b' D_{s0} \frac{\partial C}{\partial x} \frac{\partial}{\partial x} \left(\frac{1}{(1+b'C)^2} \right) \quad (7)$$

The last term in equation (7) can be written as

$$\frac{\partial}{\partial x} \left(\frac{1}{(1+b'C)^2} \right) = \left(\frac{-b'}{1+b'C} \right) \frac{\partial C}{\partial x} \quad (8)$$

Thus, we consequently obtain:

$$\left[\phi + \frac{(1-\phi) C_{\mu s} b'}{(1+b'C)^2} \right] \frac{\partial C}{\partial t} = \frac{1}{x^2} \frac{\partial}{\partial x} \left(\phi D_p x^2 \frac{\partial C}{\partial x} \right) + \frac{C_{\mu s} b'}{(1+b'C)^2} \frac{1}{x^2} \frac{\partial}{\partial x} \left[(1-\phi) D_{s0} x^2 \frac{\partial C}{\partial x} \right] - \frac{(1-\phi) C_{\mu s} b'^2 D_{s0}}{1+b'C} \left(\frac{\partial C}{\partial x} \right)^2 \quad (9)$$

The quadratic concentration gradient term of equation (9) is negligibly small, therefore it is safe to ignore. Further, ϕD_p and $(1-\phi) D_{s0}$ terms are assumed to be independent of concentration and do not change in space and time. Thus, we obtain

$$\left[\phi + \frac{(1-\phi) C_{\mu s} b'}{(1+b'C)^2} \right] \frac{\partial C}{\partial t} = \phi D_p \frac{1}{x^2} \frac{\partial}{\partial x} \left(x^2 \frac{\partial C}{\partial x} \right) + \frac{(1-\phi) C_{\mu s} b' D_{s0}}{(1+b'C)^2} \frac{1}{x^2} \frac{\partial}{\partial x} \left[x^2 \frac{\partial C}{\partial x} \right] \quad (10)$$

Now, equation (10) could be re-organized such that it has the structure of equation (3) and, hence, yielding an apparent diffusion coefficient described in terms of the intrinsic macropore and solid diffusion coefficients as:

$$D = \frac{D_p + \left(\frac{1-\phi}{\phi} \right) \left(\frac{\partial C_\mu}{\partial C} \right) D_{s0}}{1 + \left(\frac{1-\phi}{\phi} \right) \left(\frac{\partial C_\mu}{\partial C} \right)} = \frac{D_p + \left(\frac{1-\phi}{\phi} \right) \left(\frac{C_{\mu s} b'}{(1+b'C)^2} \right) D_{s0}}{1 + \left(\frac{1-\phi}{\phi} \right) \left(\frac{C_{\mu s} b'}{(1+b'C)^2} \right)} \quad (11)$$

Consequently, and in conclusion, an expression for the effective diffusion coefficient is obtained as a measure of the overall gas transport in the bidisperse particle. Due to the influence of adsorption in the microporous solid, however, the coefficient is concentration-dependent; hence, it varies in space and time. Once an initial boundary value problem is defined and a solution is obtained to equation (10) in terms of free methane concentration in the macropores, the effective diffusion coefficient could be easily investigated with respect to a fixed macropore diffusion coefficient using:

$$\frac{D}{D_p} = \frac{1 + \left(\frac{1-\phi}{\phi} \right) \left(\frac{C_{\mu s} b'}{(1+b'C)^2} \right) \left(\frac{D_{s0}}{D_p} \right)}{1 + \left(\frac{1-\phi}{\phi} \right) \left(\frac{C_{\mu s} b'}{(1+b'C)^2} \right)} \quad (12)$$

Below, transformation of the described theoretical problem into a dimensionless form by scaling of the quantities and nondimensionalization of the governing equation is explained.

2.1 Scaling and Non-dimensionalization

Once the following dimensionless quantities are defined,

$$c = \frac{C}{C_0}, \quad c_\mu = \frac{C_\mu}{C_{\mu 0}}, \quad r = \frac{x}{R}, \quad \tau = \frac{\delta_1 D_p t}{R^2},$$

$$\delta_1 = \frac{1}{1 + \left(\frac{C_{\mu 0}}{C_0} \right) \left(\frac{1-\phi}{\phi} \right)}, \quad \delta_2 = 1 - \delta_1,$$

$$\varepsilon = \left(\frac{C_{\mu 0}}{C_0} \right) \left(\frac{1-\phi}{\phi} \right) \left(\frac{D_{s0}}{D_p} \right),$$

dimensionless forms of equation (1) and (12) are obtained as follows:

$$\delta_1 \frac{\partial c}{\partial \tau} + \delta_2 \frac{\partial c_\mu}{\partial \tau} = \frac{1}{r^2} \frac{\partial}{\partial r} \left(r^2 \frac{\partial c}{\partial r} \right) + \frac{\varepsilon}{r^2} \frac{\partial}{\partial r} \left(r^2 \frac{\partial c_\mu}{\partial r} \right), \quad (13)$$

$$\frac{D}{D_p} = \frac{\delta_1 (1 + \lambda c)^2 + \varepsilon (1 + \lambda)}{\delta_1 (1 + \lambda c)^2 + \delta_2 (1 + \lambda)} \quad (14)$$

Here, δ_1 (δ_2) is the free (adsorbed phase) gas storage capacity of the macropores (microporous solid) with respect to the total capacity of bidisperse coal particle, and ε is a measure of the intensity of gas mass flux in the solid with respect to the flux in the macropores. The equilibrium adsorption isotherm given by equation (2) is nondimensionalized using a quantity λ which represents the isotherm nonlinearity:

$$\lambda = b' C_0 \quad (15)$$

$$c_\mu = \frac{(1 + \lambda) c}{1 + \lambda c} \quad (16)$$

Equation (16) yields the following relationships:

$$\frac{\partial c_\mu}{\partial \tau} = g(c, \lambda) \frac{\partial c}{\partial \tau} \quad \text{and} \quad \frac{\partial c_\mu}{\partial r} = g(c, \lambda) \frac{\partial c}{\partial r} \quad (17)$$

where $g(c, \lambda) = 1 + \lambda / (1 + \lambda c)^2$ represents gradient of concentration in the adsorbed phase with respect to free gas concentration. Now, equation (13) is re-arranged so that dimensionless macropore concentration c is the only dependent variable of the dimensionless governing equation:

$$(\delta_1 + \delta_2 g) \frac{\partial c}{\partial \tau} = \frac{1}{r^2} \frac{\partial}{\partial r} \left[r^2 (1 + \varepsilon g) \frac{\partial c}{\partial r} \right] \quad (18)$$

Note that with this formulation, we can easily investigate gas diffusion in bidisperse coal particle, i.e., the full problem, along with two limiting cases that could be of help during our analysis:

Case 1: Unipore diffusion model ($\varepsilon=0$, $\delta_2=0$). The system dynamics in this case is solely controlled by macropore diffusion. Adsorption and diffusion mechanisms are negligible in the microporous solid; namely, resistances due to the presence of microporous solid are not allowed. Under these specified conditions, equations (14) and (18) reduce to the following simple form:

$$\frac{D}{D_p} = 1; \quad \frac{\partial c}{\partial \tau} = \frac{D}{r^2} \frac{\partial}{\partial r} \left(r^2 \frac{\partial c}{\partial r} \right) \quad (19)$$

Case 2: Unipore adsorption/diffusion model ($\varepsilon=0$). Diffusive gas mass transport in the microporous solid is neglected; hence, no resistance due to diffusion in the solid is allowed. Consequently, adsorption is considered to take place instantaneously and mass transport is controlled only by macropore diffusion. Equation (14) and (18) in this case simplify to

$$\frac{D}{D_p} = \frac{\delta_1 (1 + \lambda c)^2}{\delta_1 (1 + \lambda c)^2 + \delta_2 (1 + \lambda)} \quad (20)$$

$$\delta_1 \frac{\partial c}{\partial \tau} + \delta_2 \frac{\partial c_\mu}{\partial \tau} = \frac{D}{r^2} \frac{\partial}{\partial r} \left(r^2 \frac{\partial c}{\partial r} \right)$$

3. Binary Diffusion in Bidisperse Coal Particle

In this section, we consider development of a theoretical model representing binary gas mixture adsorption/diffusion behavior within the same coal particle presented in §2. Now, the gas-solid system contains two coupled governing equations for components 1 and 2:

$$\begin{aligned} \phi \frac{\partial C_1}{\partial t} + (1 - \phi) \frac{\partial C_{\mu 1}}{\partial t} &= \frac{1}{x^2} \frac{\partial}{\partial x} \left(\phi D_{p1} x^2 \frac{\partial C_1}{\partial x} \right) \\ &+ \frac{1}{x^2} \frac{\partial}{\partial x} \left((1 - \phi) D_{11} x^2 \frac{\partial C_{\mu 1}}{\partial x} \right) + \frac{1}{x^2} \frac{\partial}{\partial x} \left((1 - \phi) D_{12} x^2 \frac{\partial C_{\mu 2}}{\partial x} \right) \\ \phi \frac{\partial C_2}{\partial t} + (1 - \phi) \frac{\partial C_{\mu 2}}{\partial t} &= \frac{1}{x^2} \frac{\partial}{\partial x} \left(\phi D_{p2} x^2 \frac{\partial C_2}{\partial x} \right) \\ &+ \frac{1}{x^2} \frac{\partial}{\partial x} \left((1 - \phi) D_{22} x^2 \frac{\partial C_{\mu 2}}{\partial x} \right) + \frac{1}{x^2} \frac{\partial}{\partial x} \left((1 - \phi) D_{21} x^2 \frac{\partial C_{\mu 1}}{\partial x} \right) \end{aligned} \quad (21)$$

Consistent with the nomenclature of single-component case, C_1 , C_2 and $C_{\mu 1}$, $C_{\mu 2}$ represent concentrations of the gas mixture components in the macro- and micropores, respectively. D_{p1} and D_{p2} are the macropore diffusion coefficient for each component, which will be fixed to constant average values throughout the work. D_{11} and D_{22} are

the main term and D_{12} and D_{21} are the cross-term diffusion coefficients in the solid phase, which will be explicitly described later by equation (24) and (25). Equations in (21) could be written in a form similar to equation (1):

$$\begin{aligned} \phi \frac{\partial C_1}{\partial t} + (1 - \phi) \frac{\partial C_{\mu 1}}{\partial t} &= \\ \frac{1}{x^2} \frac{\partial}{\partial x} \left(\phi D_{p1} x^2 \frac{\partial C_1}{\partial x} \right) &+ \frac{1}{x^2} \frac{\partial}{\partial x} \left((1 - \phi) D_{s1} x^2 \frac{\partial C_{\mu 1}}{\partial x} \right) \end{aligned} \quad (22)$$

$$\begin{aligned} \phi \frac{\partial C_2}{\partial t} + (1 - \phi) \frac{\partial C_{\mu 2}}{\partial t} &= \\ \frac{1}{x^2} \frac{\partial}{\partial x} \left(\phi D_{p2} x^2 \frac{\partial C_2}{\partial x} \right) &+ \frac{1}{x^2} \frac{\partial}{\partial x} \left((1 - \phi) D_{s2} x^2 \frac{\partial C_{\mu 2}}{\partial x} \right) \end{aligned}$$

where D_{s1} and D_{s2} are diffusion coefficients for the components in the microporous solid represented as:

$$D_{s1} = D_{11} + D_{12} \frac{\partial C_{\mu 2} / \partial r}{\partial C_{\mu 1} / \partial r}; \quad D_{s2} = D_{22} + D_{21} \frac{\partial C_{\mu 1} / \partial r}{\partial C_{\mu 2} / \partial r} \quad (23)$$

Here, the main and cross-term diffusion coefficients are dependent on concentrations of the adsorbed components and the single-component solid diffusion coefficients D_{10} and D_{20} as follows:

$$\begin{aligned} D_{11} &= \frac{C_m - C_{\mu 2}}{C_m - C_{\mu 1} - C_{\mu 2}} \\ &+ \alpha (D_{s10} D_{s20})^{1/2} \frac{(C_{\mu 1} C_{\mu 2})^{1/2}}{C_m - C_{\mu 1} - C_{\mu 2}} \end{aligned} \quad (24)$$

$$\begin{aligned} D_{22} &= \frac{C_m - C_{\mu 1}}{C_m - C_{\mu 1} - C_{\mu 2}} \\ &+ \alpha (D_{s10} D_{s20})^{1/2} \frac{(C_{\mu 1} C_{\mu 2})^{1/2}}{C_m - C_{\mu 1} - C_{\mu 2}} \end{aligned}$$

$$\begin{aligned} D_{12} &= \frac{C_{\mu 1}}{C_m - C_{\mu 1} - C_{\mu 2}} \\ &+ \alpha (D_{s10} D_{s20})^{1/2} \left(\frac{C_{\mu 1}}{C_{\mu 2}} \right)^{1/2} \frac{C_m - C_{\mu 1}}{C_m - C_{\mu 1} - C_{\mu 2}} \end{aligned} \quad (25)$$

$$\begin{aligned} D_{21} &= \frac{C_{\mu 2}}{C_m - C_{\mu 1} - C_{\mu 2}} \\ &+ \alpha (D_{s10} D_{s20})^{1/2} \left(\frac{C_{\mu 2}}{C_{\mu 1}} \right)^{1/2} \frac{C_m - C_{\mu 2}}{C_m - C_{\mu 1} - C_{\mu 2}} \end{aligned}$$

In equations (24) and (25) α is the so-called lateral molecular interaction coefficient for binary solid diffusion. $\alpha = +1$ corresponds to co-diffusion of the components in the adsorbed phase; whereas $\alpha = -1$ to their counter-diffusion. C_m , on the other hand, represents an average saturation concentration for the mixture in the microporous solid:

$$\frac{1}{C_m} = \frac{c_{\mu 10}}{C_{m1}} + \frac{c_{\mu 20}}{C_{m2}} \quad (26)$$

Hence, it is influenced by saturation concentrations C_{m1} and C_{m2} and dimensionless initial concentrations $c_{\mu 10}$ and $c_{\mu 20}$ of the adsorbed components in the solid:

$$c_{\mu 10} = \frac{C_{\mu 10}}{C_{\mu 10} + C_{\mu 20}} \quad \text{and} \quad c_{\mu 20} = \frac{C_{\mu 20}}{C_{\mu 10} + C_{\mu 20}}$$

We consider that the binary gas mixture obeys the multi-component Langmuir adsorption isotherm. Hence,

$$C_{\mu 1} = \frac{C_m b_1' C_1}{1 + b_1' C_1 + b_2' C_2} \quad \text{and} \quad C_{\mu 2} = \frac{C_m b_2' C_2}{1 + b_1' C_1 + b_2' C_2} \quad (27)$$

However, quantitative analysis of the next section will also consider deviations from this ‘‘Langmuirian’’ behavior by taking into account the adsorbed phase molecular interaction in the range $-1 < \alpha < 1$. The latter corresponds to the existence of lateral molecular interactions between the adsorbed molecules in the microporous solid. Equations in (27) can be used to estimate concentration gradient ratios of the components in the adsorbed phase in terms of concentrations of the components in free gas in the macropores as follows:

$$\frac{\partial C_{\mu 1}}{\partial r} = \frac{\partial}{\partial r} \left(\frac{C_m b_1' C_1}{1 + b_1' C_1 + b_2' C_2} \right) = \left[\frac{C_m b_1' C_1 + C_m b_1' b_2' C_2}{(1 + b_1' C_1 + b_2' C_2)^2} \right] \frac{\partial C_1}{\partial r} - \left[\frac{C_m b_1' b_2' C_1}{(1 + b_1' C_1 + b_2' C_2)^2} \right] \frac{\partial C_2}{\partial r} \quad (28a)$$

$$\frac{\partial C_{\mu 2}}{\partial r} = \frac{\partial}{\partial r} \left(\frac{C_m b_2' C_2}{1 + b_1' C_1 + b_2' C_2} \right) = \left[\frac{C_m b_2' C_1 + C_m b_1' b_2' C_1}{(1 + b_1' C_1 + b_2' C_2)^2} \right] \frac{\partial C_2}{\partial r} - \left[\frac{C_m b_1' b_2' C_2}{(1 + b_1' C_1 + b_2' C_2)^2} \right] \frac{\partial C_1}{\partial r} \quad (28b)$$

ratio of which gives

$$\frac{\partial C_{\mu 1} / \partial r}{\partial C_{\mu 2} / \partial r} = \frac{(b_1' + b_1' b_2' C_2) \frac{\partial C_1}{\partial r} - (b_1' b_2' C_1) \frac{\partial C_2}{\partial r}}{(b_2' + b_1' b_2' C_1) \frac{\partial C_2}{\partial r} - (b_1' b_2' C_2) \frac{\partial C_1}{\partial r}} \quad (29)$$

Then, the solid diffusion coefficients of the components (i.e., equations in 23) could be written as

$$D_{s1} = D_{11} + D_{12} \frac{(b_2' + b_1' b_2' C_1) \frac{\partial C_2}{\partial r} - (b_1' b_2' C_2) \frac{\partial C_1}{\partial r}}{(b_1' + b_1' b_2' C_2) \frac{\partial C_1}{\partial r} - (b_1' b_2' C_1) \frac{\partial C_2}{\partial r}} \quad (30)$$

$$D_{s2} = D_{22} + D_{21} \frac{(b_1' + b_1' b_2' C_2) \frac{\partial C_1}{\partial r} - (b_1' b_2' C_1) \frac{\partial C_2}{\partial r}}{(b_2' + b_1' b_2' C_1) \frac{\partial C_2}{\partial r} - (b_1' b_2' C_2) \frac{\partial C_1}{\partial r}}$$

3.1 Scaling and Non-dimensionalization

Similar to the single-component case, we define the following dimensionless quantities for the binary case:

$$c_1 = \frac{C_1}{C_{10} + C_{20}}, \quad c_{\mu 1} = \frac{C_{\mu 1}}{C_{\mu 10} + C_{\mu 20}}, \quad c_2 = \frac{C_2}{C_{10} + C_{20}},$$

$$c_{\mu 2} = \frac{C_{\mu 2}}{C_{\mu 10} + C_{\mu 20}}, \quad r = \frac{x}{R}, \quad \tau = \frac{\delta_1 D_{p1} t}{R^2} = \frac{\delta_1 D_{p2} t}{R^2} \left(\frac{D_{s20}}{D_{s10}} \right),$$

$$\delta_1 = \frac{1}{1 + \left(\frac{1 - \phi}{\phi} \right) \left(\frac{C_{\mu 10} + C_{\mu 20}}{C_{10} + C_{20}} \right)}, \quad \delta_2 = 1 - \delta_1$$

$$\varepsilon_1 = \left(\frac{C_{\mu 10} + C_{\mu 20}}{C_{10} + C_{20}} \right) \left(\frac{1 - \phi}{\phi} \right) \left(\frac{D_{s1}}{D_{s10}} \right) \left(\frac{D_{s10}}{D_{p1}} \right)$$

$$\varepsilon_2 = \left(\frac{C_{\mu 10} + C_{\mu 20}}{C_{10} + C_{20}} \right) \left(\frac{1 - \phi}{\phi} \right) \left(\frac{D_{s2}}{D_{s20}} \right) \left(\frac{D_{s20}}{D_{p2}} \right)$$

$$\lambda_1 = b_1' (C_{10} + C_{20}), \quad \lambda_2 = b_2' (C_{10} + C_{20}).$$

Hence, the governing equations (22) and (27) in dimensionless form are

$$\delta_1 \frac{\partial c_1}{\partial \tau} + \delta_2 \frac{\partial c_{\mu 1}}{\partial \tau} = \frac{1}{r^2} \frac{\partial}{\partial r} \left(r^2 \frac{\partial c_1}{\partial r} \right) + \frac{1}{r^2} \frac{\partial}{\partial r} \left(r^2 \varepsilon_1 \frac{\partial c_{\mu 1}}{\partial r} \right) \quad (31)$$

$$\delta_1 \frac{\partial c_2}{\partial \tau} + \delta_2 \frac{\partial c_{\mu 2}}{\partial \tau} = \frac{1}{r^2} \frac{\partial}{\partial r} \left(r^2 \frac{\partial c_2}{\partial r} \right) + \frac{1}{r^2} \frac{\partial}{\partial r} \left(r^2 \varepsilon_2 \frac{\partial c_{\mu 2}}{\partial r} \right)$$

and

$$c_{\mu 1} = \frac{(1 + \lambda_1 + \lambda_2) c_1}{1 + \lambda_1 c_1 + \lambda_2 c_2}; \quad c_{\mu 2} = \frac{(1 + \lambda_1 + \lambda_2) c_2}{1 + \lambda_1 c_1 + \lambda_2 c_2} \quad (32)$$

Again, using the chain rule, the accumulation terms on the left hand sides of the equations in (31) can be written in terms of concentrations of the free gas in the macropores:

$$\frac{\partial c_{\mu 1}}{\partial \tau} = g_1 \frac{\partial c_1}{\partial \tau} - g_1' \frac{\partial c_2}{\partial \tau}$$

$$\frac{\partial c_{\mu 2}}{\partial \tau} = g_2 \frac{\partial c_2}{\partial \tau} - g_2' \frac{\partial c_1}{\partial \tau}$$

where we define

$$g_1(c_1, c_2) = \frac{(1 + \lambda_1 + \lambda_2)(1 + \lambda_2 c_2)}{(1 + \lambda_1 c_1 + \lambda_2 c_2)^2}$$

$$g_2(c_1, c_2) = \frac{(1 + \lambda_1 + \lambda_2)(1 + \lambda_1 c_1)}{(1 + \lambda_1 c_1 + \lambda_2 c_2)^2} \quad (33)$$

$$g_1'(c_1, c_2) = \frac{(1 + \lambda_1 + \lambda_2) \lambda_2 c_1}{(1 + \lambda_1 c_1 + \lambda_2 c_2)^2}$$

$$g_2'(c_1, c_2) = \frac{(1 + \lambda_1 + \lambda_2) \lambda_1 c_2}{(1 + \lambda_1 c_1 + \lambda_2 c_2)^2}$$

Similarly, the right hand sides of equations in (31) are written as

$$\frac{1}{r^2} \frac{\partial}{\partial r} \left(r^2 \frac{\partial c_1}{\partial r} \right) + \frac{1}{r^2} \frac{\partial}{\partial r} \left(r^2 \varepsilon_1 \frac{\partial c_{\mu 1}}{\partial r} \right) = \frac{1}{r^2} \frac{\partial}{\partial r} \left(r^2 \frac{\partial c_1}{\partial r} \right) + \frac{1}{r^2} \frac{\partial}{\partial r} \left[r^2 \varepsilon_1 g_1 \frac{\partial c_1}{\partial r} \right] - \frac{1}{r^2} \frac{\partial}{\partial r} \left[r^2 \varepsilon_1 g_1' \frac{\partial c_2}{\partial r} \right] \quad (34)$$

$$\frac{1}{r^2} \frac{\partial}{\partial r} \left(r^2 \frac{\partial c_2}{\partial r} \right) + \frac{1}{r^2} \frac{\partial}{\partial r} \left(r^2 \varepsilon_2 \frac{\partial c_{\mu 2}}{\partial r} \right) =$$

$$\frac{1}{r^2} \frac{\partial}{\partial r} \left(r^2 \frac{\partial c_2}{\partial r} \right) + \frac{1}{r^2} \frac{\partial}{\partial r} \left[r^2 \varepsilon_2 g_2 \frac{\partial c_2}{\partial r} \right] - \frac{1}{r^2} \frac{\partial}{\partial r} \left[r^2 \varepsilon_2 g_2' \frac{\partial c_1}{\partial r} \right]$$

These expansions give equations in (31) in a compact dimensionless form as follows:

$$\begin{aligned}
& (\delta_1 + \delta_2 g_1) \frac{\partial c_1}{\partial \tau} - (\delta_2 g_1') \frac{\partial c_2}{\partial \tau} = \\
& \frac{1}{r^2} \frac{\partial}{\partial r} \left[r^2 (1 + \varepsilon_1 g_1) \frac{\partial c_1}{\partial r} \right] - \frac{1}{r^2} \frac{\partial}{\partial r} \left(r^2 \varepsilon_1 g_1' \frac{\partial c_2}{\partial r} \right)
\end{aligned} \tag{35}$$

$$\begin{aligned}
& (\delta_1 + \delta_2 g_2) \frac{\partial c_2}{\partial \tau} - (\delta_2 g_2') \frac{\partial c_1}{\partial \tau} = \\
& \frac{1}{r^2} \frac{\partial}{\partial r} \left[r^2 (1 + \varepsilon_2 g_2) \frac{\partial c_2}{\partial r} \right] - \frac{1}{r^2} \frac{\partial}{\partial r} \left(r^2 \varepsilon_2 g_2' \frac{\partial c_1}{\partial r} \right)
\end{aligned}$$

which could be further simplified into

$$\begin{aligned}
& \left(\delta_1 + \delta_2 g_1 - \delta_2 g_1' \frac{\partial c_2}{\partial c_1} \right) \frac{\partial c_1}{\partial \tau} = \\
& \frac{1}{r^2} \frac{\partial}{\partial r} \left[r^2 \left(1 + \varepsilon_1 g_1 - \varepsilon_1 g_1' \frac{\partial c_2}{\partial c_1} \right) \frac{\partial c_1}{\partial r} \right]
\end{aligned} \tag{36a}$$

$$\begin{aligned}
& \left(\delta_1 + \delta_2 g_2 - \delta_2 g_2' \frac{\partial c_1}{\partial c_2} \right) \frac{\partial c_2}{\partial \tau} = \\
& \frac{1}{r^2} \frac{\partial}{\partial r} \left[r^2 \left(1 + \varepsilon_2 g_2 - \varepsilon_2 g_2' \frac{\partial c_1}{\partial c_2} \right) \frac{\partial c_2}{\partial r} \right]
\end{aligned} \tag{36b}$$

Note that equations (36a) and (36b) are similar in form to equation (18) of the single-component case, except that the parameters ε_1 and ε_2 now include normalized binary solid diffusion coefficients which are not constant but given explicitly in dimensionless form:

$$\frac{D_{s1}}{D_{s10}} = \left(\frac{D_{11}}{D_{s10}} \right) + \left(\frac{D_{12}}{D_{s10}} \right) \frac{\left(\lambda_1 + \lambda_1 \lambda_2 c_2 \right) \frac{\partial c_1}{\partial r} - \lambda_1 \lambda_2 c_1 \frac{\partial c_2}{\partial r}}{\left(\lambda_2 + \lambda_1 \lambda_2 c_1 \right) \frac{\partial c_1}{\partial r} - \lambda_1 \lambda_2 c_2 \frac{\partial c_1}{\partial r}} \tag{37}$$

$$\frac{D_{s2}}{D_{s20}} = \left(\frac{D_{22}}{D_{s20}} \right) + \left(\frac{D_{21}}{D_{s20}} \right) \frac{\left(\lambda_2 + \lambda_2 \lambda_1 c_1 \right) \frac{\partial c_2}{\partial r} - \lambda_1 \lambda_2 c_2 \frac{\partial c_1}{\partial r}}{\left(\lambda_1 + \lambda_2 \lambda_1 c_2 \right) \frac{\partial c_1}{\partial r} - \lambda_1 \lambda_2 c_1 \frac{\partial c_2}{\partial r}}$$

with the main diffusion coefficients D_{11} and D_{22} are now described explicitly as

$$\frac{D_{11}}{D_{s10}} = (1 + \lambda_1 c_1) + \alpha \left(\frac{D_{s20}}{D_{s10}} \right)^{1/2} (\lambda_1 \lambda_2 c_1 c_2)^{1/2} \tag{38}$$

$$\frac{D_{22}}{D_{s20}} = (1 + \lambda_2 c_2) + \alpha \left(\frac{D_{s10}}{D_{s20}} \right)^{1/2} (\lambda_1 \lambda_2 c_1 c_2)^{1/2}$$

and the cross-term coefficients D_{12} , D_{21} as

$$\frac{D_{12}}{D_{s10}} = \lambda_1 c_1 + \alpha \left(\frac{D_{s20}}{D_{s10}} \right)^{1/2} \left(\frac{\lambda_1 c_1}{\lambda_2 c_2} \right)^{1/2} (1 + \lambda_2 c_2) \tag{39}$$

$$\frac{D_{21}}{D_{s20}} = \lambda_2 c_2 + \alpha \left(\frac{D_{s10}}{D_{s20}} \right)^{1/2} \left(\frac{\lambda_2 c_2}{\lambda_1 c_1} \right)^{1/2} (1 + \lambda_1 c_1)$$

Here, prior to analysis of the dimensionless governing equations, an understanding of the lateral molecular interaction coefficient α is required. Consider co-diffusion of the gas components in the bidisperse coal particle where α takes positive values. As it can be

seen from equations (38) and (39), mass fluxes of the gas components in this case reach to a maximum when $\alpha = +1$; their values decrease with α and eventually reach to a minimum when $\alpha = 0$. Chen and Yang [10] showed that $\alpha = +1$ corresponds to the case when there are no lateral interaction between the adsorbed molecules in the microporous solid, i.e., mixed Langmuirian-type adsorption. Then, it follows that the lateral molecular interaction in the adsorbed phase decreases the fluxes, hence, slow down mass transport of the gas components from the microporous solid to the macropores. In the following, we follow a comparative investigation in §5.2 and consider three cases during the analysis:

Case 3: Binary diffusion in microporous solid with maximum lateral molecular interaction ($\alpha = 0$)

Case 4: Co-diffusion in microporous solid with no lateral molecular interaction ($\alpha = +1$)

Case 5: Counter-diffusion in microporous solid with no lateral molecular interaction ($\alpha = -1$)

4. Numerical Method

Equations (18), (19), (20) and (36) describe transient gas transport in bidisperse coal particle in terms of the free gas concentrations (c ; c_1 and c_2) in the macropores. Equation (19) is linear; whereas the others are nonlinear parabolic equations, numerical approximations of which could be obtained using an implicit finite difference scheme and Newton iteration. Developed numerical scheme of this work considers several initial-boundary value problems that will be described below. The scheme uses an accurate second order spatial discretization method on a fixed set of nodes specified by the user. Time integration of the ordinary differential equations resulting from the discretization in space is performed by an ode solver which is based on an implicit linear multi-step method that chooses the time steps dynamically during the computations [12].

5. Results and Discussion

5.1 Methane Diffusion in the Coal Particle

In this section, we consider methane release from the described bidisperse coal particle and look for unique solutions to equations (18), (19) and (20) using the following initial and boundary conditions:

$$\begin{aligned}
\tau = 0 & ; c(r, 0) = 1 \\
r = 0 & ; \partial c / \partial r = 0 \\
r = 1 & ; c = 0
\end{aligned} \tag{40}$$

Methane is initially distributed uniformly as free gas in the macropores and in an adsorbed state in the microporous solid dictated by the equilibrium adsorption isotherm. Since the outer boundary condition (at $r=1$) is described as a sink for methane, there should be diffusive transport of the free gas in the macropores as well as gas desorption and diffusion in the solid. Note that the conditions are defined for the free methane concentration in the macropores, although concentration of the adsorbed methane at any particular time and location could be easily computed using equation (16).

Table 1.
Parameters for Gas Adsorption/Diffusion
in Bidisperse Coal Particle

Parameter	Value	Range
Macroporosity (ϕ)	5%	1-9%
$C_{\mu s}$ (methane) mol/ cm ³	2.0E-3	0.5 - 3.0E-3
$C_{\mu s}$ (CO ₂) mol/ cm ³	3.0E-3	1.5 - 3.5E-3
b' (methane) cm ³ /mole	500	400-600
b' (CO ₂) cm ³ /mole	1200	1000-1400
C_0 mol/ cm ³	1.6E-3	1.0 - 2.5E-3
$\lambda = b'C_0$ (methane)	0.80	0.40-1.5
$\lambda = b'C_0$ (CO ₂)	1.92	1-3.5
$C_{\mu 0}/C_0 = C_{\mu s}b'/(1 + \lambda)$ (methane)	0.5	0.14-0.52
$C_{\mu 0}/C_0 = C_{\mu s}b'/(1 + \lambda)$ (CO ₂)	1.03	0.75-1.09
D_{s0}/D_p ; D_{s10}/D_{p1} ; D_{s20}/D_{p2}	1.0E-2	<< 0.1
δ_1	0.078	0.067-0.148

These conditions also imply that the film diffusion resistance is negligible at the external surface of coal particle.

A sensitivity analysis is performed in the following pages for the described methane recovery problem using base values for the model parameters listed in **Table 1**. The analysis includes influences of the macroporosity, ϕ , the surface diffusion coefficient, D_{s0} , the initial amount and distribution of methane in the macropores and in the solid, $C_{\mu 0}/C_0$, and the influences of Langmuir isotherm through the parameters, $C_{\mu s}$ and b . Due to the nature of full problem, we will perform the analysis in time at a fixed location close to the center of the coal particle, $r=0.1$.

Figure 1 shows results and compares with the unipore diffusion model (case 1), see dotted and solid lines with $\phi=0.01$, respectively, in terms of the free methane gas concentration profile (Figure 1a) and the rate of methane recovery (Figure 1c). Free gas in the macropores is estimated to be recovered approximately within an hour, whereas, complete recovery of methane in the adsorbed phase takes nearly 40 hours. Thus, the microporous solid undisputedly plays the role of a barrier during the gas release, significantly increasing the time duration for methane recovery.

The Effect of Macroporosity. Figure 1 also shows the methane/coal particle system behavior for varying ϕ in terms of the estimated free and adsorbed methane concentrations (Figures 1a and 1b), of the methane mole fraction recovered (Figure 1c) and of the effective diffusion coefficient (Figure 1d). Overall the observed trends clearly indicate the importance of microporous solid volume available for methane adsorption. As the solid volume of the coal particle is increased, i.e., ϕ decreased, mole fraction of the initially distributed adsorbed methane in the solid increases. Consequently, longer time durations are required to release the same amount of methane from the solid phase. For example, Figure 1c shows that the time for complete methane recovery increases about 4 times as the macroporosity is varied from 5 to 1 per cent.

Interestingly, the estimated diffusion coefficient values deviate drastically from the unipore model, with $D=1.0$, where both adsorption and surface diffusion are ignored (Figure 1d). Its value drops significantly during an early transition period, during when the

free gas in macropores is released, and stabilizes to a constant low value prior to the complete methane recovery. Note that the duration of transient period increases with the microporous solid volume. Further, at large volumes, for example when $\phi=0.01$, the stabilized value of effective diffusivity with respect to the macropore diffusivity is as low as $D/D_p=2/100$.

The Effect of Surface Diffusion. Comparisons of the results with the second unipore model, which includes instantaneous gas desorption and release from the micropores (case 2, dashed line), shows an additional 20% drop in the stabilized effective diffusivity value. This drop is solely due to the presence of surface diffusion in the microporous solid. **Figure 2**, however, shows that this influence is not amplified as the surface diffusion coefficient is further decreased. The latter indicates the existence of nonlinearity given by equation (12) between the effective diffusion coefficient and free gas concentration. Thus, although surface diffusion could create a resistance; mainly, it is the retardation due to adsorption in microporous solid that controls the methane recoveries from the bidisperse coal particle.

The Effect of Initially Available Methane in Bidisperse Coal Particle. Similarly, **Figure 3** illustrates the system behavior in time for varying $C_{\mu 0}/C_0$ ratio. Note that, in this case, volume fraction of the microporous solid is fixed; instead, initial concentration of free and adsorbed methane in the coal particle is varied. Figure 3a and 3b shows that the total amount of initially available methane in the particle decreases with the increasing ratio. This means that we are not only investigating the influence of an increasing concentration contrast (adsorbed/free), but also a decrease in the initially available total gas amount. Figure 3c shows that the time it takes for a complete methane recovery does not change significantly, see the elapse times in Figures 1c for $\phi=0.05$ and compare with and 3c. It is, however, conclusive that methane recovery occurs much slower due to increasing contrast, even though the initial total gas amount becomes less. This indicates the importance of initial methane distribution in the coal particle.

As in agreement with Figures 1d and 2, we observe similar trends in the estimated effective methane diffusion coefficient: a characteristic transition period with a sharp decrease in its value, followed by a late-time period with a constant stabilized value. Initial value of the coefficient approaches to unity (i.e., case 1), as more gas becomes available in the macropores. Regardless of the ratio, the time for a stabilized coefficient is nearly the same; it reaches a constant value of $D/D_p=6/100$ at about 4 hours.

The Effects of Adsorption Isotherm. This part of the analysis deals with the nature of gas to be released from the coal particle. The isotherm parameters are varied such that direct comparisons with CO₂ release could be made. **Figure 4** shows the influence of $C_{\mu s}$, i.e., the complete monolayer coverage. Results indicate that the adsorbed gas concentration profile is influenced by the monolayer coverage. The adsorbed CO₂ concentration is larger in the solid phase, regardless of the particle location. However, the rate of gas recovery and the complete recovery time is the same for the methane and CO₂ coverage values. The effective diffusion coefficient, on the other, further drops in the case of CO₂ release, but the estimates are still in the proximity of values with methane.

Figure 5 shows that, unlike the influence of monolayer coverage, the Langmuir constant b , i.e., the isotherm nonlinearity, has a significant impact on the gas release rate from the particle. Since CO₂ has a larger adsorption capacity with the coal, i.e., large b value,

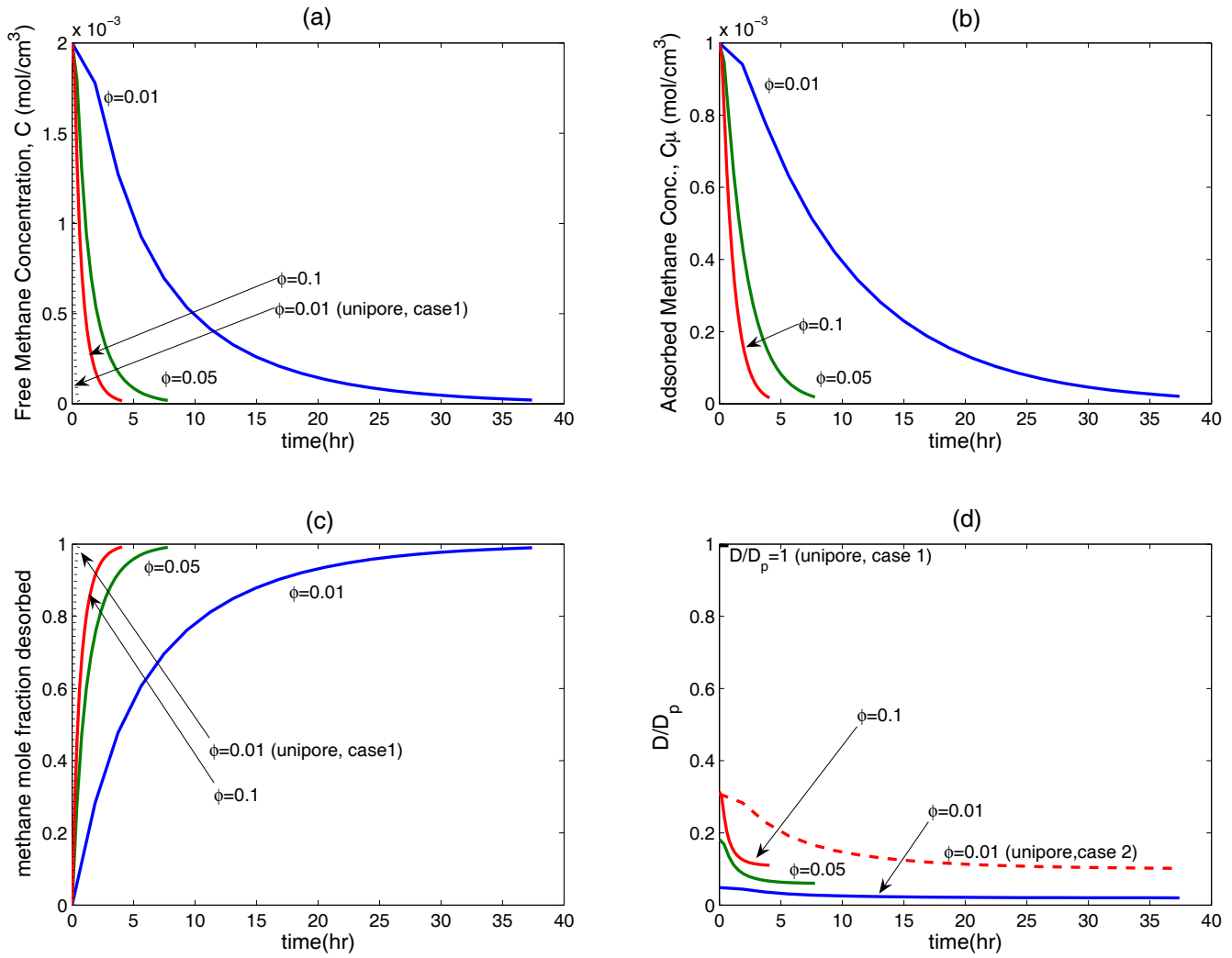


Figure 1. Effect of macroporosity. $r=0.1$, $D_p/R^2=3.0E-4$ 1/s, $C_{\mu}/C_o=0.5$, $b=500$ cc/mol, $C_{\mu}=2.0E-3$ mole/cc, $D_s/D_p=0.01$. Dashed lines represent solutions with the unipore models given by equations (16) and (17)

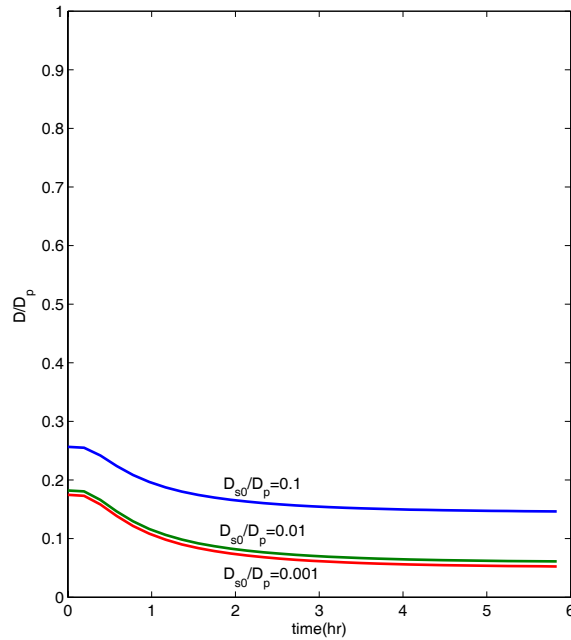


Figure 2. Effect of solid diffusion. $r=0.1$, $D_p/R^2=3.0E-4$ 1/s, $\phi=0.05$, $C_{\mu}/C_o=0.5$, $b=500$ cc/mol, $C_{\mu}=2.0E-3$ mole/cc.

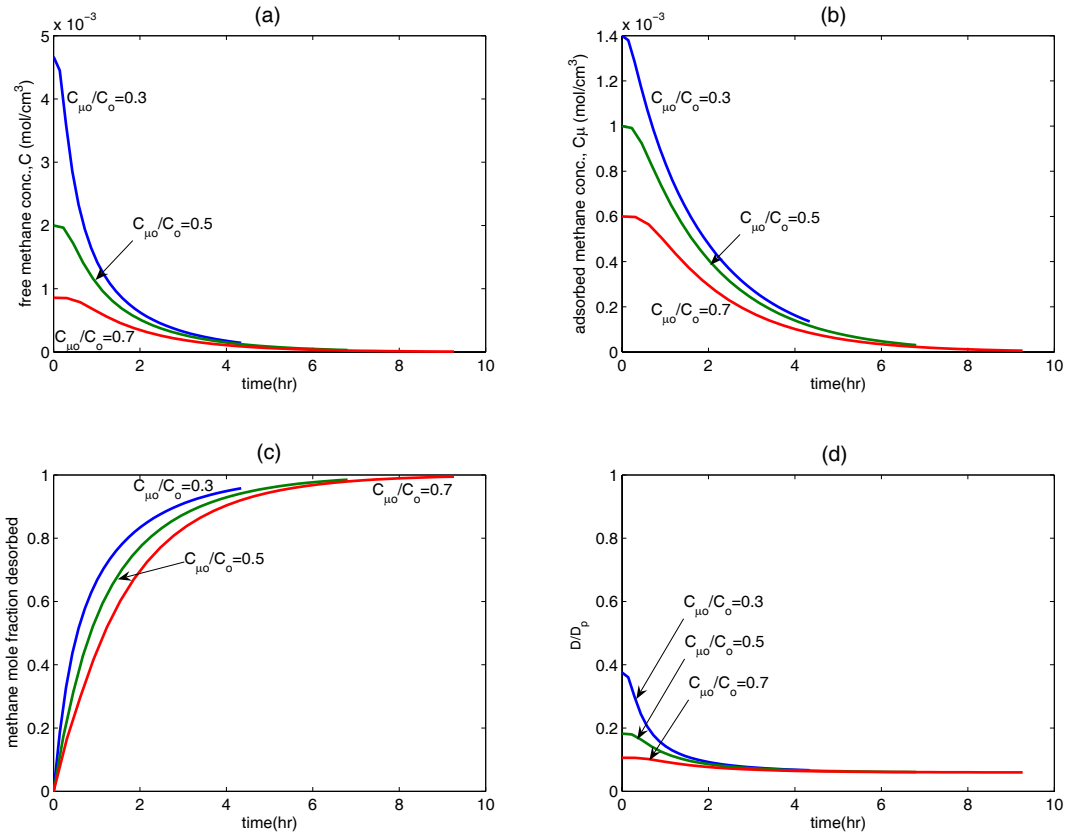


Figure 3. Single Component Diffusion: Effect of initial methane amount and distribution. $r=0.1$, $D_p/R^2=3.0E-4$ 1/s, $\phi=0.05$, $b=500$ cc/mol, $C_{\mu s}=2.0E-3$ mole/cc, $D_s/D_p=0.01$.

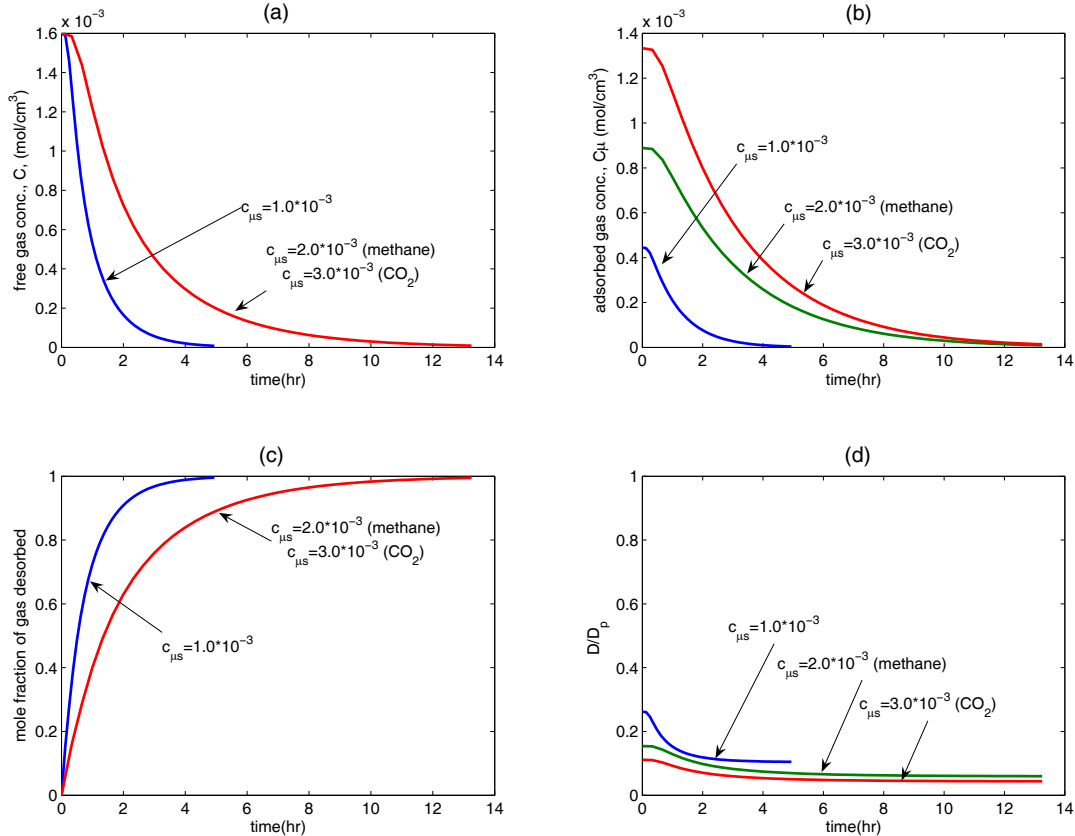


Figure 4. Single Component Diffusion: Effect of complete monolayer coverage. $r=0.1$, $D_p/R^2=3.0E-4$ 1/s, $\phi=0.05$, $b=500$ cc/mol, $C_{\mu s}/C_o=0.5$, $D_s/D_p=0.01$.

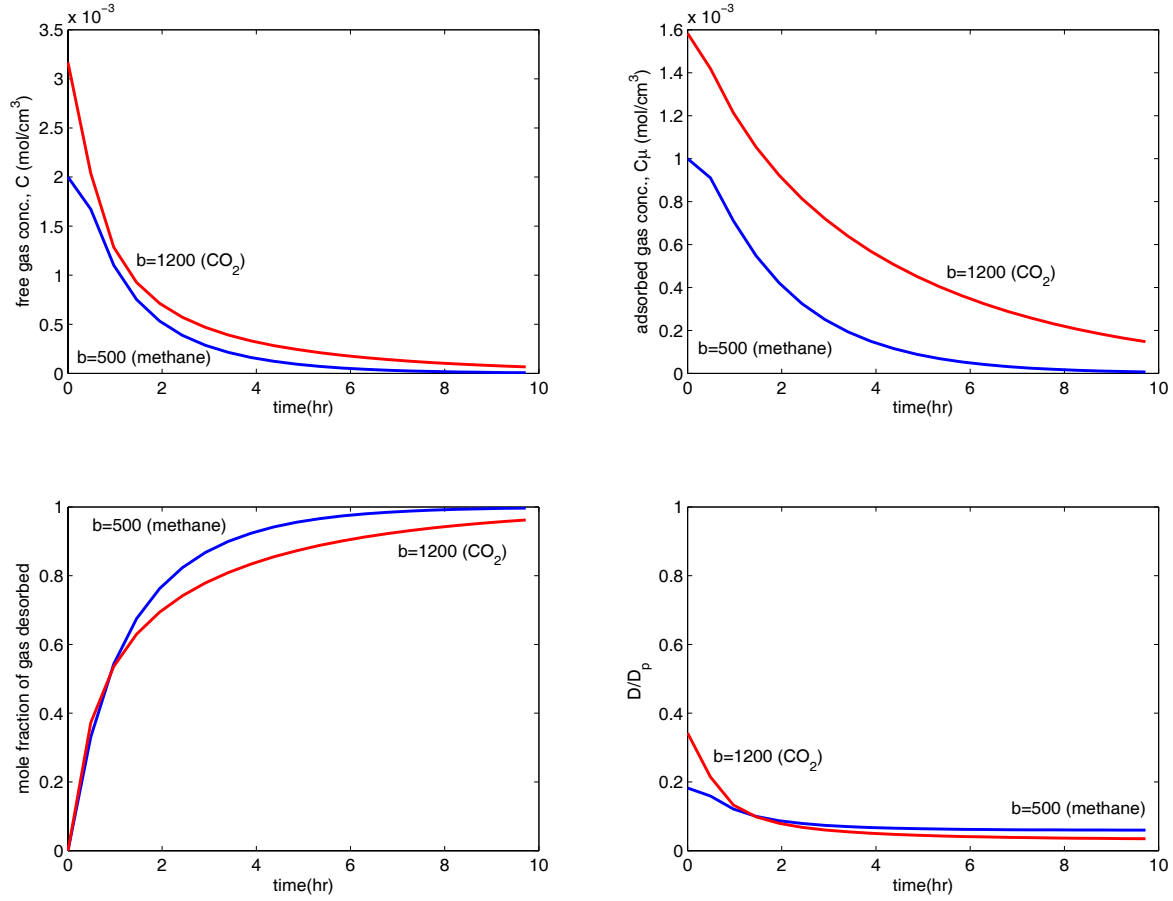


Figure 5. Single Component Diffusion: Effect of Langmuir isotherm constant. $r=0.1$, $D_p/R^2=3.0E-4$ 1/s, $\phi=0.05$, $C_{\mu}=2.0E-3$ mole/cc, $C_{\mu}/C_o=0.5$, $D_s/D_p=0.01$

it takes significantly longer time duration to completely recover it. The early time recovery variations are negligible.

In summary, although the overall mass transport is influenced by the intrinsic macropore and solid diffusion coefficients, the rate of methane release is primarily controlled by methane sorption in the microporous solid. An effective diffusion coefficient of the problem is concentration dependent, hence, varies in time and space. Its value at a particular location drops significantly during an initial transition period, as the free gas in macropores is depleted, and stabilizes to a constant value prior to the complete methane recovery. Further, duration of the transient period increase dramatically with the microporous solid volume, the initially adsorbed methane concentration in the solid and D_{s0}/D_p ratio. Next, the analysis is extended to methane-CO₂ mixtures under varying conditions in the coal particle.

5.2 Methane/CO₂ Co-diffusion in the Coal Particle

In this section, solutions to the coupled equations in (36) will be considered using the following initial/boundary conditions:

$$\begin{aligned} \tau=0 & ; c_1=c_{10}; c_2=c_{20} \\ r=0 & ; \partial c_1/\partial r=0; \partial c_2/\partial r=0 \\ r=1 & ; c_1=0; c_2=0 \end{aligned} \quad (41)$$

Here the indices 1 and 2 correspond to methane and CO₂, respectively. Initially, solid phase of the coal particle is saturated with fixed concentrations (c_{10} and c_{20}) of methane and CO₂, and the solution yields the gas mixture distribution (release) in (from) the

particle in time and space. Hence, the exercise is a non-trivial one, relevant to methane behavior in coal matrices during primary CBM production in the presence of naturally occurring CO₂.

The Effect of Lateral Interactions in Microporous Solid.

Figure 6 compares the binary Langmuirian-type adsorption and the adsorption with the maximum lateral molecular interactions between the adsorbed gas molecules, i.e., $\alpha=0$ in equations (38) and (39). In the binary cases (solid lines), the coal particle is initially saturated with 5% CO₂. The fractional methane recovery curves show that, although gas release is slower when strong lateral interactions exist in the microporous solid, the time required for complete gas recovery is nearly the same. It takes slightly longer times for complete methane recovery with the maximum interactions. This observation, however, is not necessarily valid for CO₂, for which the interactions are more pronounced; consequently, the time duration for its ultimate recovery is much longer than the Langmuirian case. Further investigation is currently required to understand the level of these interactions between the adsorbed methane and CO₂ molecules in microporous coals. Here, the results clearly show that transport and recovery of the component with larger adsorption capacity is retarded in the presence of lateral molecular interactions in microporous solids. During the rest of the analysis, for simplicity, we consider Langmuir adsorption and, hence, take $\alpha=\pm 1.0$.

Methane-CO₂ Co-diffusion Coefficients in Microporous Solid.

Figure 6 also compares these fractional curves to the one with single-component case, shown with the dashed lines. Note the marked difference in methane recoveries in the presence of CO₂. Although

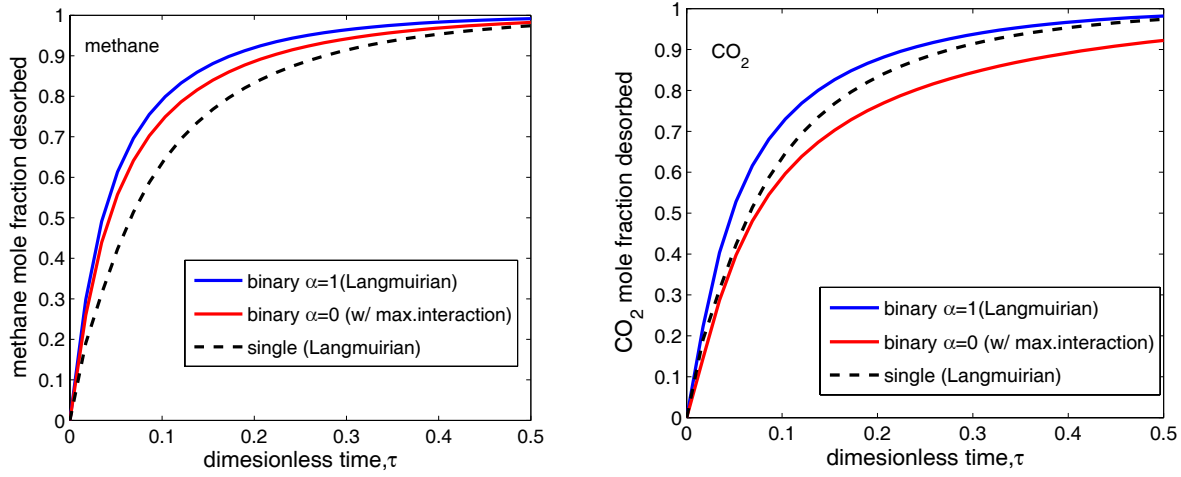


Figure 6. Comparison of single-component and binary diffusion (Cases 3 and 4) in bidisperse coal particle: Fractional recovery curves for methane and CO₂. Initially available CO₂ concentration is 5%.

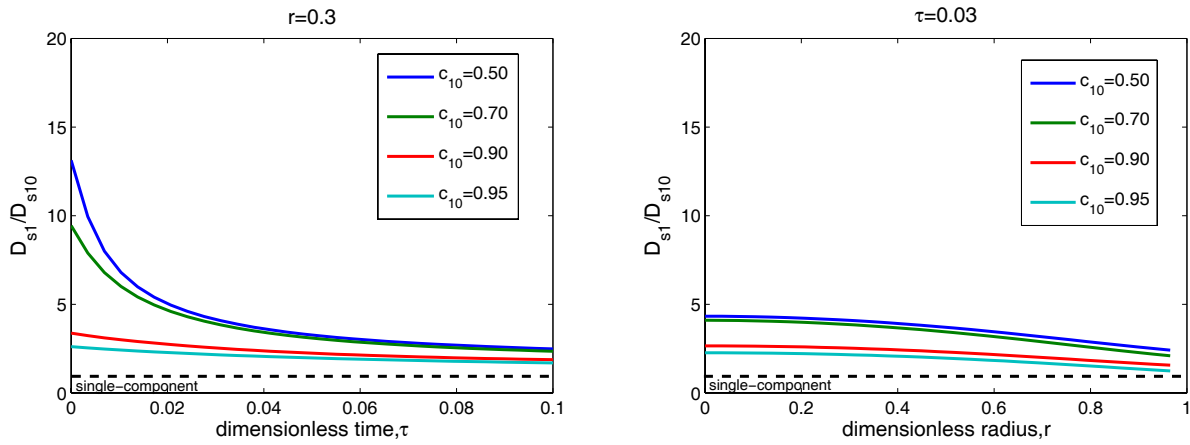


Figure 7. Methane and CO₂ co-diffusion (Case 4) in bidisperse coal particle: Effect of initial gas mixture concentrations on methane diffusion coefficient in microporous solid. Initially available CO₂ concentration in the coal particle is increased 5, 10, 30 and 50%.

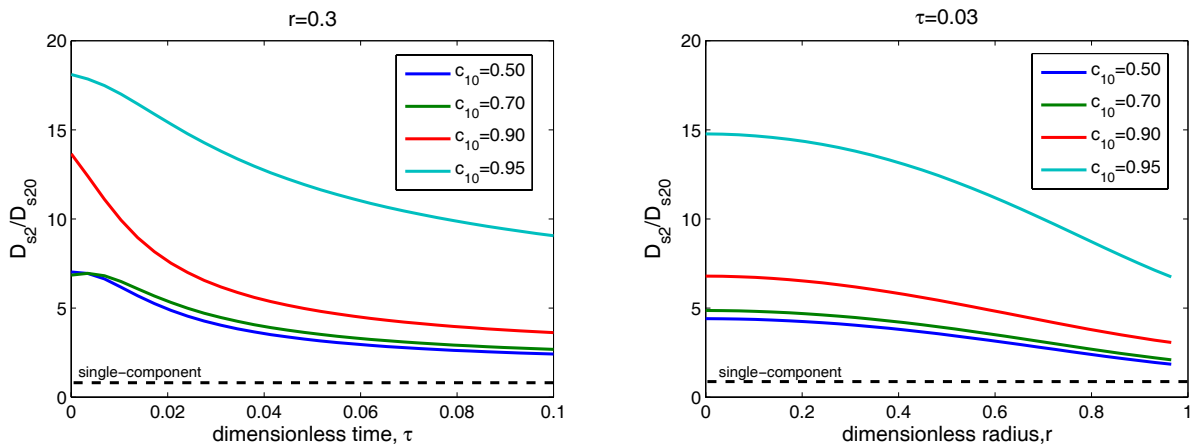


Figure 8. Methane and CO₂ co-diffusion (Case4) in bidisperse coal particle: Effect of initial gas mixture concentrations on CO₂ diffusion coefficient in microporous solid. Initially available CO₂ concentration in the coal particle is increased 5, 10, 30 and 50%.

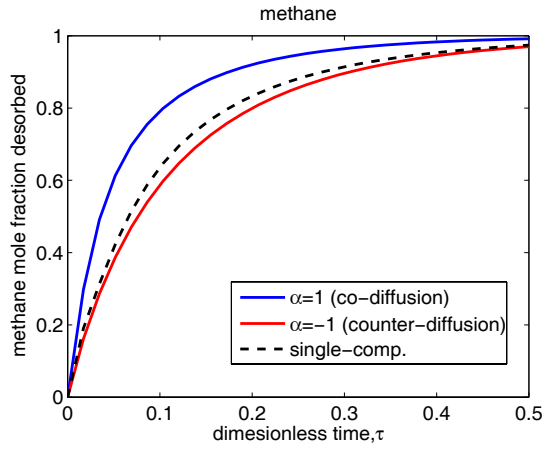


Figure 9. Comparison of single-component methane desorption with cases 3 ($\alpha=0$), 4 (co-diffusion) and 5 (counter-diffusion): Fractional recoveries from bidisperse coal particle. Initially available CO_2 concentration in the coal particle is 5%.

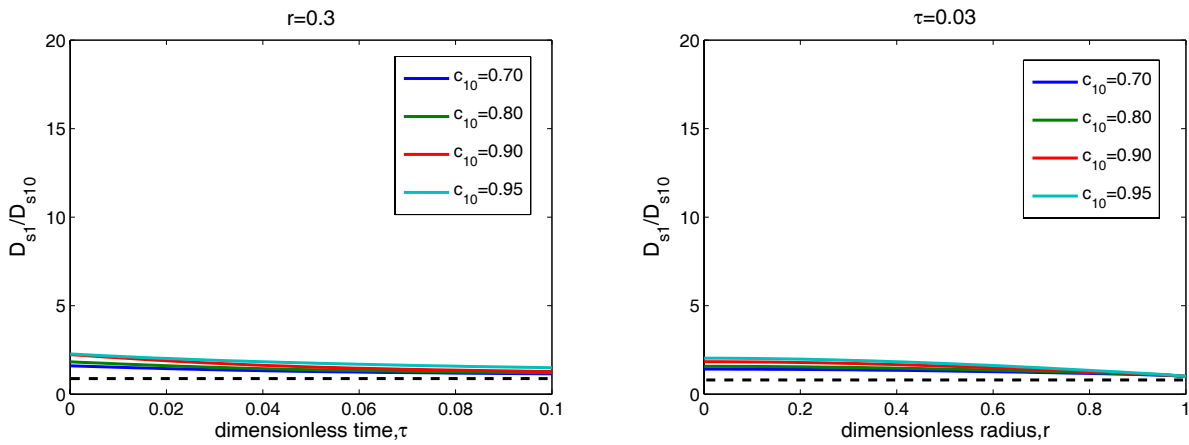


Figure 10. Methane and CO_2 counter-diffusion (Case 5) in bidisperse coal particle: Effect of initial gas mixture concentrations on methane diffusion coefficient in microporous solid. Initially available CO_2 concentration in the coal particle is increased 5, 10, 20 and 30%.

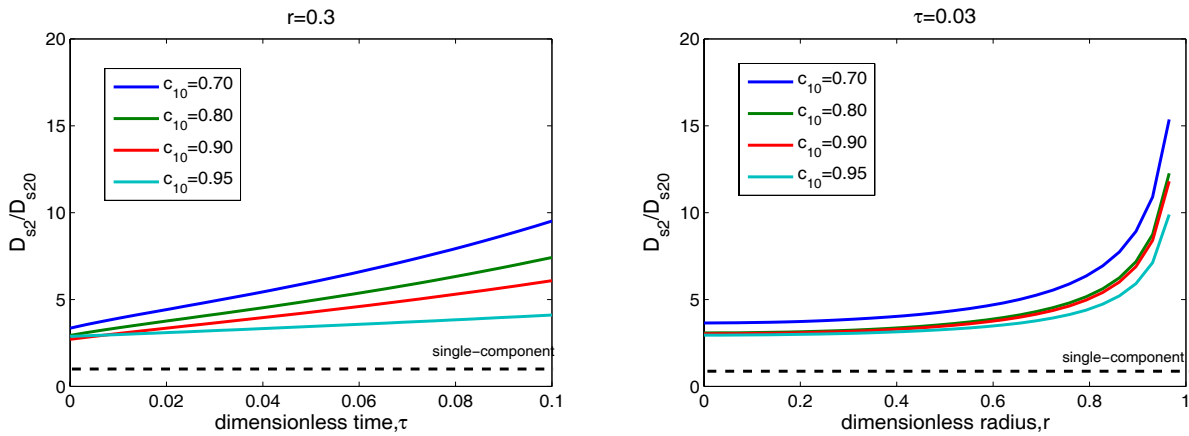


Figure 11. Methane and CO_2 counter-diffusion (Case5) in bidisperse coal particle: Effect of initial gas mixture concentrations on CO_2 diffusion coefficient in microporous solid. Initially available CO_2 concentration in the coal particle is increased 5, 10, 20 and 30%.

methane is still dominantly present in the microporous solid, it is transported together with CO₂ in the micropores at a larger rate; consequently, its recovery, as well as the recovery of CO₂, is significantly improved. Co-diffusion of the gas mixture has, therefore, a positive impact on the transport of both of the components.

Next, co-diffusion coefficients in the microporous solid are investigated for varying initial concentrations of CO₂. **Figure 7** shows that the estimated diffusion coefficient for methane transport in micropores increases with the initial CO₂ concentrations, in particular during early transient and at radial locations closer to the center of the coal particle. The increase, however, is not as satisfactory as in the case of CO₂ transport coefficient, for which much larger values are estimated in **Figure 8**. Solid diffusion coefficient for the latter, for example with a 5% initial concentration, is 4-6 times larger than the one for methane. Interestingly, in contrary to the methane case, the CO₂ diffusion coefficient appears to be decreasing as its initial concentration in the coal particle is increased. This is in contrast to what one would intuitively expect and shows an intricate interplay of selective adsorption and co-diffusion in the microporous solid.

5.3 Methane/CO₂ Counter-diffusion in the Coal Particle

In this section, solutions to equation (36) will be considered using the following initial/boundary conditions:

$$\begin{aligned} \tau=0 & ; c_1=1.0; c_2=0 \\ r=0 & ; \partial c_1/\partial r=0; \partial c_2/\partial r=0 \\ r=1 & ; c_1=0; c_2=1.0 \end{aligned} \quad (42)$$

Initially, the coal particle is saturated with methane only and the gas mixture behavior is investigated in space and time under fixed outer boundary conditions, i.e., a constant sink/source of methane/CO₂. Hence, the exercise resembles methane and CO₂ behavior in the coal matrices during a CO₂-ECBM process.

Fractional Methane Recovery. **Figure 9** compares the estimated fractional methane recoveries of three problems: single-component (methane only) diffusion, binary co-diffusion and counter-diffusion (initially 5% CO₂). It is clear that in the case of counter-diffusion the incoming CO₂ molecules plays the role of a barrier during the methane release and, hence, the estimated fractional values in this case is significantly less than the values for co- and single-component diffusion.

Methane-CO₂ Counter-diffusion Coefficients in Microporous Solid. The counter effect is also clear in **Figure 10** where the predicted methane diffusion coefficient is small and much closer to its value with the single-component case (compare Figures 7 and 10). Also in contrary to the co-diffusion case, an increase in initially available CO₂ concentration appears to have only a negligible effect on the estimated coefficient values. **Figure 11** shows the estimated CO₂ diffusion coefficient in the micropores during counter-diffusion. As in the co-diffusion case, the coefficient is much larger with respect to the coefficient for methane. It increases in time, as more CO₂ invades the particle, and in space, in particular, closer to the outer boundary where its concentration is much larger. Note that, in the counter-diffusion case, the estimated CO₂ diffusion coefficient increases with its initial concentration in the particle.

In summary, it is found that the methane transport in microporous solids improves and its release from the solid is promoted in the presence CO₂, regardless of the direction of transport

of the latter. The improvement is amplified when both components have fluxes in the same direction; whereas, it is damped when they are in reverse direction. Indeed, a better understanding of the gas-particle dynamics could be gained when an investigation is performed using effective diffusion coefficients that reflect the transport of components both in the macropores and microporous solid, which is discussion of the next section.

5.4 Methane-CO₂ Effective Diffusion in Coal Particle – Role of Micropores on Binary Gas Transport

The effective methane and CO₂ diffusion coefficients in bidisperse coal particle are from equations (36a) and (36b):

$$\begin{aligned} D_{eff1} &= I + \varepsilon_1(g_1 - g'_1 dc_2/dc_1) \\ D_{eff2} &= I + \varepsilon_2(g_2 - g'_2 dc_1/dc_2) \end{aligned} \quad (43)$$

These equations are dimensionless and include (1) the macropore and microporous solid diffusion mechanisms in quantity 1.0 and parameters ε_i , respectively; and (2) the influence of binary

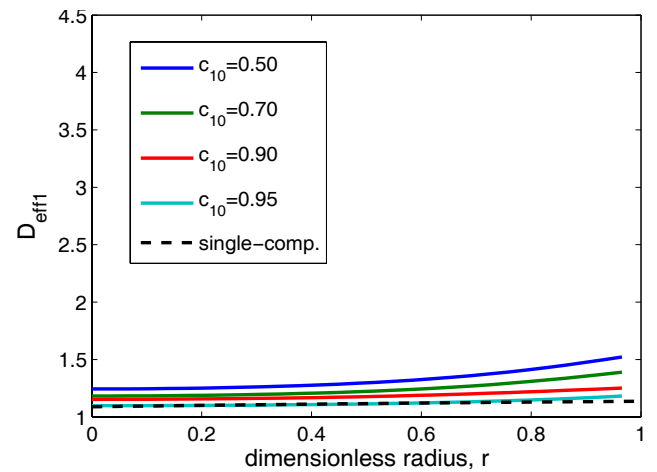


Figure 12. Methane and CO₂ co-diffusion (Case 4) in bidisperse coal particle: Influence of initial gas mixture concentrations on effective methane diffusion coefficient in the coal particle. Initially available CO₂ concentration in the coal particle is increased 5, 10, 30 and 50%.

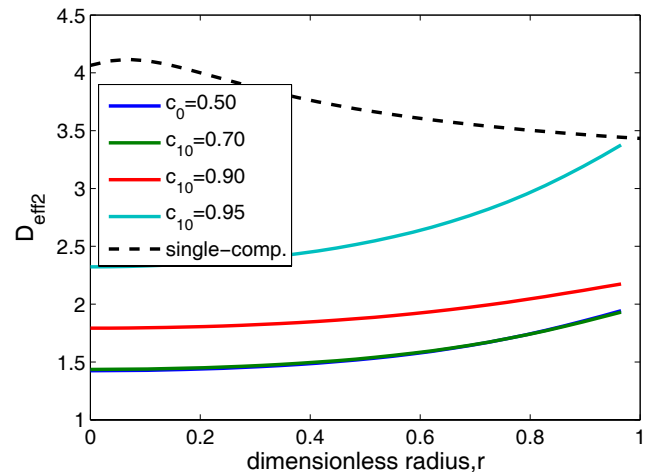


Figure 13. Methane and CO₂ co-diffusion in bidisperse coal particle (Case 4): Influence of initial gas mixture concentrations on effective CO₂ diffusion coefficient in the coal particle. Initially available CO₂ concentration in the coal particle is increased 5, 10, 30 and 50%.

equilibrium adsorption in the parenthesis terms. Hence, influences of competitive adsorption and diffusion mechanisms in microporous solid are the product term in the equations and appear as deviations from unity, i.e. macropore diffusion.

Figures 12 shows the estimated effective co-diffusion coefficients for methane in the bidisperse coal particle at a fixed time. (The trends at a fixed location are similar in varying time). It is clear that the estimates are always larger than 1.0, namely, the gas transport is overall enhanced by the component-component and component-solid interactions in the micropores. The enhancement in overall methane transport is not of significant importance near the particle center, although it is more pronounced closer to the outer boundary, which plays the role of a sink for both components. Recall that, in §5.2 a significant improvement is reported for methane transport in the microporous solid: the estimated values of its diffusion coefficient are as large as 5-15 near the center and drops to values in the range of 3-5 near the particle boundary, see Figure 7. The analysis of this section, however, indicates that those co-diffusion improvements in the values of ε_I are partially compensated by binary adsorption in microporous solid, i.e., the parenthesis term in (43); therefore, they appear as rather small deviations from unity for the estimated overall methane transport coefficient.

The same discussion is also valid for CO₂ during co-diffusion, the overall transport coefficient of which is shown in **Figure 13**. The latter also shows that, although adsorption retards this component as well, the micropore diffusion effects are relatively more pronounced at any location in the particle.

In essence, binary adsorption mechanism creates an additional retardation effect during the gas mass transport of the components in microporous solid. Further, a delicate balance exists between binary diffusion and adsorption in the microporous solid during gas recoveries from the coal particle. In the case of methane, outcome of this balance creates a relatively small fluctuation during its transport in the macropores; whereas, in the case of CO₂, it becomes rather noticeable.

Figure 14 shows the effective methane transport coefficient during counter-diffusion in the bidisperse coal particle. It appears that the coefficient is nearly as large as the macropore diffusion coefficient; hence, the product terms of equation (43) has negligible effect on methane transport at any location in the particle during counter diffusion of the components. The effective transport coefficient of CO₂, on the other hand, has values on the order of 1.0. **Figure 15** shows that it increases near the outer boundary indicating strong micropore diffusion effects in that region.

6. Concluding Remarks

Theoretical framework presented here considers presence of microporous solids in coalbed matrices; emphasizes their role as the places to retain majority of the gas; and investigates their role in gas transport and storage during CBM and CO₂-ECBM processes. The approach recognizes bimodal pore structure of the matrices, i.e., macro- and micropores: it introduces the pore structure to the framework in a simple mathematical form that defines gas mass accumulation and flux terms for each mode. Then the single-component and binary mixture gas/solid interactions are rigorously investigated considering initial-boundary value problems in 1-D spherical coordinate and using an implicit finite difference scheme.

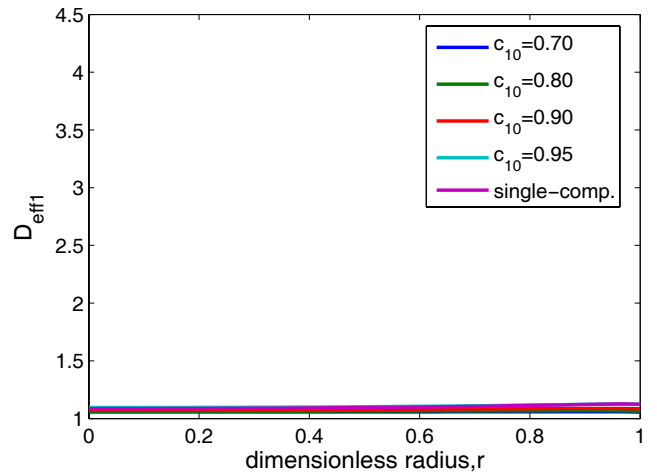


Figure 14. Methane and CO₂ counter-diffusion (Case 5) in bidisperse coal particle: Effect of initial gas mixture concentrations on effective methane diffusion coefficient in the coal particle. Initially available CO₂ concentration in the coal particle is increased 5, 10, 20 and 30%.

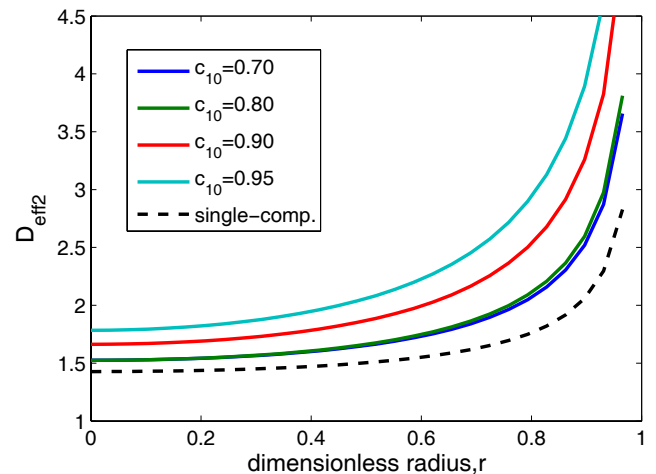


Figure 15. Methane and CO₂ counter-diffusion (Case 5) in bidisperse coal particle: Effect of initial gas mixture concentrations on effective CO₂ diffusion coefficient in the coal particle. Initially available CO₂ concentration in the coal particle is increased 5, 10, 20 and 30%.

It is found that the fractional volume of microporous solid plays a crucial role during the gas transport: initially it distributes a larger fraction of gas in the solid in a physically adsorbed state. Recovery of the latter is then limited by diffusion and equilibrium adsorption in the solid. It is found that binary gas transport is improved due to presence of same-direction mass fluxes; however, the improvement could be masked significantly by retardation effect of the adsorption.

The approach could be easily modified for rectangular geometries representing the coal matrices and incorporated into currently used conventional simulators. Nevertheless, 1-D spherical models of this work appear to be suitable for further fundamental investigations dealing with other important components of the same problem such as the influences of macropore flow, stress and pore pressure, or water on overall transport in the matrix.

Acknowledgement

This research was partially funded by Natural Science Foundation of Chongqing (CNSFC), China, and by the Natural Science and Engineering Research Council of Canada (NSERC). Here, we gratefully acknowledge their financial contributions.

NOMENCLATURE

c = nondimensional macropore concentration
 c_{μ} = nondimensional micropore concentration
 b = Langmuir isotherm constant (cm^3/mol)
 C = macropore concentration (mol/cm^3)
 C_o = initial macropore concentration (mol/cm^3)
 $C_{\mu o}$ = sorbed concentration in equilibrium with C_o (mol/cm^3)
 C_{μ} = microporous solid-phase concentration (mol/cm^3)
 $C_{\mu s}$ = maximum sorbed-phase concentration in Langmuir isotherm (mol/cm^3)
 D = apparent diffusion coefficient (cm^2/s)
 D_s = micropore (solid) diffusion coefficient (cm^2/s)
 D_p = macropore diffusion coefficient (cm^2/s)
 R = radius of coal particles (cm)
 r = nondimensional radial coordinate
 t = real time coordinate
 x = dimensional radial coordinate

Greek symbols

τ = nondimensional time
 λ = dimensionless Langmuir isotherm nonlinearity parameters
 ϕ = macroporosity
 ε = ratio of sorbed phase to macropore flux
 δ_1 = nondimensional macropore capacity
 δ_2 = nondimensional microporous solid phase capacity

REFERENCES

1. THIMONS, E.D., KISSELL, F.N., "Diffusion of Methane through Coal," *Fuel Vol. 52*, 274–280, 1973.
2. KARACAN, C. O., "An Effective Method for Resolving Spatial Distribution of Adsorption Kinetics in Heterogeneous Porous Media: Application for Carbon dioxide Sequestration in Coal," *Chemical Engineering Science, Vol. 58*, 4681-4693, 2003.
3. CLARKSON C.R., BUSTIN, R.M., "The Effect of Pore Structure and Gas Pressure upon the Transport Properties of Coal: A Laboratory and Modelling Study. 2. Adsorption Rate Modelling," *Fuel Vol. 78*, 1345–1362, 1999.
4. RUCKENSTEIN, E., VAIDYANATHAN, A.S. and YOUNGQUIST, G.R., "Sorption by Solids with Bidisperse Pore Structures," *Chem. Eng. Sci.*, Vol. 26, 1305-1318 1971.
5. SMITH, D.M. and WILLIAMS, F.L., "Diffusion Models for Gas Production from Coal - Determination of Diffusion Parameters," *Fuel Vol. 63*, 256–261, 1984.
6. SHI, J.Q. and DURUCAN S., "A Bidisperse Pore Diffusion Model for Methane Displacement and Desorption in Coal by CO_2 Injection," *Fuel, Vol. 82, No 11*, 1219, 2003.
7. GRAY, P.G. and DO, D. D., "A Graphical Method for Determining Pore and Surface Diffusivities in Adsorption Systems," *Ind. Eng. Chem. Res.*, Vol. 31, 1176-1182, 1992.
8. CUSSLER, E.L., "Multicomponent Diffusion," *Elsevier, Amsterdam*, 1976.
9. KRISHNA, R., "Multicomponent Surface Diffusion of Adsorbed Species: A Description Based on the Generalized Maxwell-Stefan Equations," *Chem. Eng. Sci. Vol. 45* 1779-1791, 1990.
10. CHEN, Y.D. and YANG, R.T., "Predicting Binary Fickian Diffusivities from Pure Component Diffusivities for Surface Diffusion," *Chem. Eng. Sci. Vol. 47 No. 15/16* 3895-3905, 1992.
11. SUNDARAM, N. and YANG, R.T., "Binary Diffusion of Unequal Sized Molecules in Zeolites," *Chem. Eng. Sci. Vol. 55* 1747-1754, 2000.
12. HIGHAM D.J. and HIGHAM, N.J., "Matlab Guide," *Society for Industrial and Applied Mathematics, Philadelphia*, 2000.